SCIENCE CHINA Chemistry



ARTICLES

https://doi.org/10.1007/s11426-025-2840-0

Fluorinated covalent organic frameworks enable photocatalytic H_2O_2 production via a photoinduced framework radical pathway

Weixue Tao¹, Yuchen Wang¹, Linghui Cong¹, Chenhui Zhang¹, Yan Gao¹, Haifeng Zheng², Wenjie Shi^{1*}, Dichang Zhong^{1*} & Tongbu Lu^{1*}

¹Institute for New Energy Materials and Low Carbon Technologies, School of Materials Science and Engineering, Tianjin University of Technology, Tianjin 300384, China

²Frontier Institute of Science and Technology, Xi'an Jiaotong University, Xi'an 710054, China

Received April 24, 2025; accepted June 13, 2025; published online August 8, 2025

Photosynthesis of hydrogen peroxide (H_2O_2) via oxygen reduction reaction (ORR) and water oxidation reaction (WOR) pathways requires controlled formation of radical intermediates. However, achieving precise control over radical formation in metalfree catalysts remains challenging. Herein, we report a fluorinated COF (Kf-F-COF) featuring framework-bound carbonyl groups as intrinsic radical-generating sites for efficient dual-channel H_2O_2 photosynthesis. This design enables the simultaneous activation of O_2 and H_2O through radical-mediated hydrogen atom transfer processes. Mechanistic studies reveal that fluorination enhances the electron affinity of the carbonyl sites, facilitates diradical formation, and lowers the energy barriers of key reaction steps. As a result, Kf-F-COF achieves a high H_2O_2 production rate of 6.42 mmol g^{-1} h^{-1} and long-term stability under natural sunlight and seawater conditions. This work presents a framework-centered radical strategy for dual-pathway H_2O_2 photosynthesis and offers mechanistic insights into regulating COF-based photocatalysts.

covalent organic frameworks, dual-channel H_2O_2 photocatalysis, framework-bound radical

Citation: Tao W, Wang Y, Cong L, Zhang C, Gao Y, Zheng H, Shi W, Zhong D, Lu T. Fluorinated covalent organic frameworks enable photocatalytic H₂O₂ production via a photoinduced framework radical pathway. Sci China Chem, 2025, 68, https://doi.org/10.1007/s11426-025-2840-0

1 Introduction

Hydrogen peroxide (H_2O_2) is an important green oxidant with wide-ranging applications across various industrial sectors [1]. Photocatalytic H_2O_2 production, which utilizes solar energy to directly convert water (H_2O) and oxygen (O_2) into H_2O_2 , offers a sustainable alternative to the conventional anthraquinone process [2,3]. Compared to the four-electron water oxidation pathway, the two-electron water oxidation and oxygen reduction pathways enhance atom economy and avoid the generation of low-value byproducts such as O_2 . [4,5]. However, realizing such a dual-pathway system re-

mains a substantial scientific and engineering challenge. According to the mechanism [6], the dual-channel synthesis of H₂O₂ proceeds via radical-mediated pathways. Therefore, the rational design of photocatalysts capable of enhancing radical generation under light irradiation offers a promising strategy to precisely regulate intermediate formation and boost the overall efficiency of H₂O₂ production.

Among various metal-free photocatalysts [7–9], covalent organic frameworks (COFs) have emerged as a promising platform to address this challenge [10–12]. COF, as a class of crystalline, porous organic materials with atomically precise architectures, offers highly designable building units and extended π -conjugated structures and favorable light-harvesting properties [13–15]. In particular, the incorporation of redox-active moieties has shown great potential in

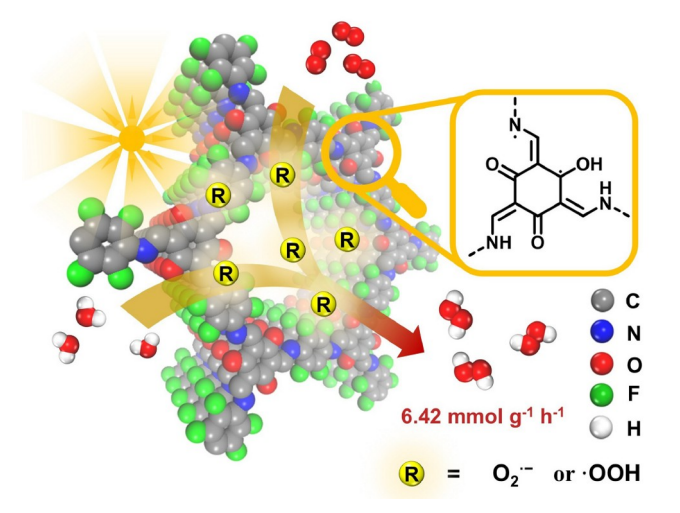
^{*}Corresponding authors (email: wjshi@email.tjut.edu.cn; dczhong@email.tjut.edu.cn; lutongbu@tjut.edu.cn)

modulating electron transfer pathways and tailoring the local electronic environment of catalytic sites [16,17]. These features grant COFs unique advantages in tuning band structures and constructing well-defined catalytic microenvironments [18,19]. Collectively, these attributes position COFs as ideal candidates for constructing well-defined, radical-active catalytic microenvironments capable of simultaneously driving ORR and WOR pathways toward efficient photocatalytic H_2O_2 production.

Herein, we present the synthesis and characterization of a fluorine-functionalized COF, Kf-F-COF, designed for efficient photosynthetic dual-channel H₂O₂ synthesis. We not only demonstrate the enhanced photocatalytic activity of Kf-F-COF but also uncover a reaction mechanism in which the carbonyl (-C=O) groups serve as photogenerated radicalactive sites. Mechanistic studies reveal that these carbonyl groups possess strong electron affinity under photoexcitation, enabling the generation and evolution of carboncentered radical intermediates. These radicals drive the activation of O₂ and H₂O through a sequence of hydrogen atom transfer (HAT) steps, culminating in the formation of H₂O₂ via both O₂ reduction and H₂O oxidation pathways. Moreover, fluorine modification is found to enhance the electron affinity of the carbonyl sites and reduce the energy barriers of key intermediate transitions, thereby significantly improving the overall catalytic performance. As a result, the Kf-F-COF achieves a high H₂O₂ production rate of 6.42 mmol g⁻¹ h⁻¹ and long-term stability under natural sunlight and seawater conditions. This mechanistic insight provides a novel perspective on designing COF-based photocatalysts for efficient H₂O₂ photosynthesis (Scheme 1).

2 Results and discussion

The fluorine-functionalized trihydroxybenzene-based COF (Kf-F-COF) was synthesized via a solvothermal method through a Schiff-base condensation reaction between 1,3,5triformylphloroglucinol (Tp) and 2,3,5,6-tetrafluoro-1,4phenylenediamine (Tfp) (Figure S1, Supporting Information online). For comparison, a non-functionalized analogue (Ef-H-COF) was synthesized using the same procedure, in which Tfp was replaced by p-phenylenediamine (Figure S2). Fourier-transform infrared (FTIR) spectroscopy confirmed the formation of both materials, showing new C-N stretching bands at 1236 cm⁻¹ for Kf-F-COF and 1233 cm⁻¹ for Ef-H-COF, while the N-H stretching bands associated with the -NH₂ groups disappeared (Figures S3 and S4) [20]. The powder X-ray diffraction (PXRD) of Kf-F-COF and Ef-H-COF agrees with simulated data, which come from the eclipsed AA stacking mode (Figure 1a and Figure S5) [21]. TEM and high-resolution transmission electron microscopy (HRTEM) images reveal a lamellar stacking structure and



Scheme 1 (Color online) Schematic illustration of the photogenerated radical-active sites in Kf-F-COF enabling dual-channel H₂O₂ photosynthesis.

excellent crystallinity for Kf-F-COF. Clear lattice fringes with a spacing of ~ 0.31 nm corresponding to π - π stacking are observed (Figure 1b), and the selected area electron diffraction pattern displays hexagonally arranged diffraction spots, confirming the ordered layered structure (Figures S6 and S7). While the Ef-H-COF presented a flower-type morphology, which indicated that the sheetlike structure of Ef-H-COF (Figure S8). Elemental mapping confirms that C, N, O, and F are uniformly distributed throughout Kf-F-COF and C, N, and O are uniformly distributed throughout Ef-H-COF (Figures S9 and S10). Solid-state ¹³C nuclear magnetic resonance (NMR) spectra confirmed that Kf-F-COF predominantly adopts a keto-form structure, with characteristic shifts at 184, 144, and 109 ppm (Figure 1c) [22,23]. In contrast, Ef-H-COF shows additional enol-form signals at 179 and 101 ppm. XPS analysis further supports the keto-form dominance in Kf-F-COF, showing a higher C-N-H content (68%) than C=N (19%) (Figure 1d, e and Figures S11–S16) [24]. All these bond ratios are higher than the Ef-H-COF, which supports the successful synthesis of an exclusive keto-form Kf-F-COF. N2 sorption measurements show that Kf-F-COF possesses a specific surface area of 293.94 m² g⁻¹ and a pore size of 1.02 nm, which is comparable to Ef-H-COF (213.13 m² g⁻¹ and 1.30 nm) (Figures S17-S20). Both COFs exhibited excellent thermal stability (Figures S21 and S22) and maintained crystallinity after solvent immersion (Figures S23 and S24). UV-vis diffuse reflectance spectroscopy (UV-vis-DRS) and Mott-Schottky (MS) analysis revealed that both Kf-F-COF and Ef-H-COF exhibit strong visible-light absorption. Notably, Kf-F-COF exhibited a broader absorption range with an edge extending to 800 nm (Figures S25 and S26). The optical bandgaps were determined to be 2.14 eV for Kf-F-COF and 2.11 eV for Ef-H-COF. MS plots indicate the conduction band minimum

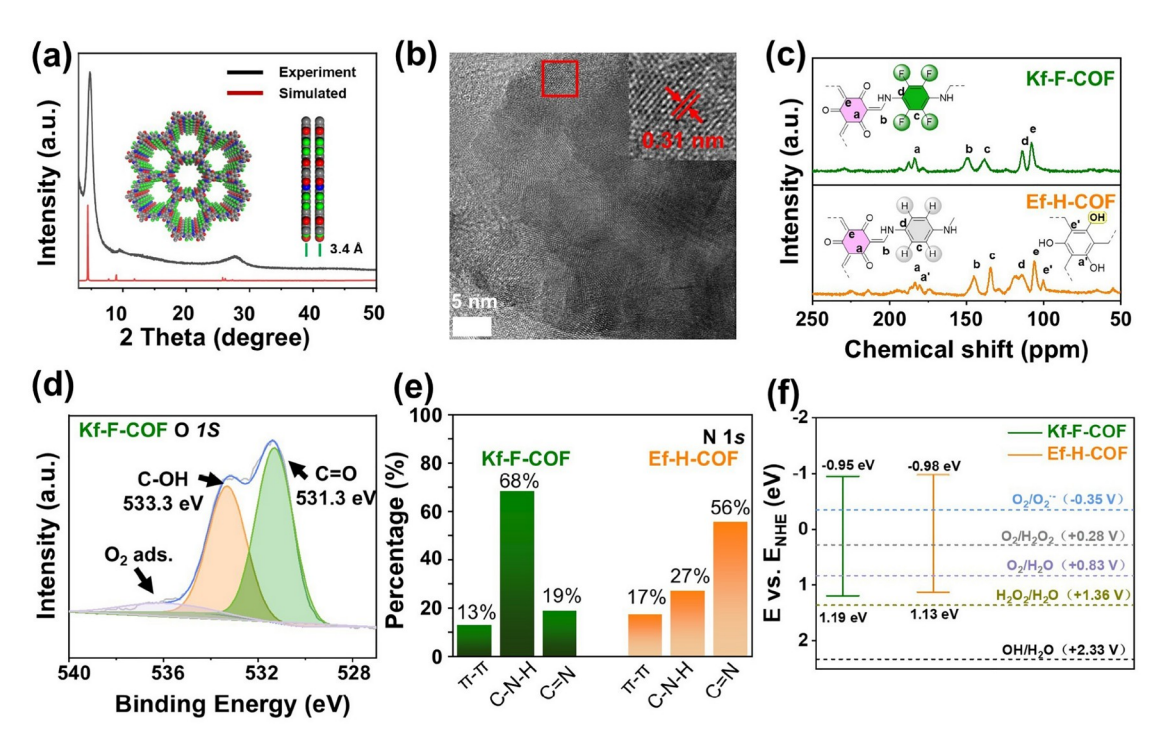


Figure 1 (Color online) Catalyst preparation and characterization. (a) Simulated (black line) and experimental (red dot) PXRD patterns of Kf-F-COF. (b) HRTEM images of Kf-F-COF. (c) Solid-state ¹³C NMR spectra of Kf-F-COF and Ef-H-COF. (d) O 1s XPS spectra of Kf-F-COF. (e) The percentage of peak areas for different chemical bonds that were calculated from the deconvoluted N 1s XPS bands. (f) Band structures of Kf-F-COF and Ef-H-COF.

(CBM) of Kf-F-COF and Ef-H-COF to be -0.95 and -0.98 V, respectively (Figures S27–S30). These band structures thermodynamically support overall photosynthesis for H_2O_2 production (Figure 1f).

Photophysical experiments were performed to evaluate the charge transport efficiency of Kf-F-COF in catalytic processes. Both Kf-F-COF and Ef-H-COF showed strong photocurrent responses (Figure S31), and Kf-F-COF presented a superior photoelectron transport ability than that of Ef-H-COF. Kf-F-COF exhibits a smaller semi-circular diameter in its Nyquist plot, suggesting enhanced charge transfer (Figure S32). In addition, the significantly quenched emission intensity and shorter excited-state lifetime of Kf-F-COF compared to Ef-H-COF imply more efficient trapping of photoexcited electrons and a suppression of charge recombination (Figures S33 and S34). Therefore, these findings confirm that the ligand modification in Kf-F-COF facilitates more effective utilization of photogenerated charges.

The photocatalytic performance of Kf-F-COF for non-sacrificial H_2O_2 production was assessed by dispersing the powder in water under pure water under an O_2 atmosphere (Figures S35 and S36). Upon visible light ($\lambda > 420$ nm), the rate of H_2O_2 production reached as high as 6.42 mmol g⁻¹ h⁻¹, which largely exceeded that of the most reported polymeric photocatalyst (Figure 2a). The H_2O_2 yield of Kf-F-COF was 17.5-fold greater than that of Ef-H-COFs (0.37 mmol g⁻¹ h⁻¹), strongly indicating the in-

dispensable role of keto-form structure in the catalyst. The catalytic performance of Kf-F-COF significantly outperforms most previously reported non-metallic COFs (Table S1 and Figure S37, Supporting Information online). The apparent quantum efficiencies (AQY) of Kf-F-COF at different wavelengths were well matched with its absorption spectrum, and the highest value appeared at 450 nm and reached 2.96% (Figure S38).

Continuous H₂O₂ production was realized using a flowtype photocatalytic converter (Figure S39). Under visible light irradiation ($\lambda > 420 \text{ nm}$) and a flow rate of 1.5 mL min⁻ with air-saturated water, the system steadily produced ~15,000 mL of H₂O₂ over 168 h (Figure 2b). Post-reaction FT-IR (Figure S40), PXRD (Figure S41), and gravimetric analysis revealed negligible structural and weight changes after the continuous flow reaction. To further demonstrate the practical applicability of Kf-F-COF, its H₂O₂ photosynthesis performance was examined under natural sunlight. Kf-F-COF efficiently produces H₂O₂ under natural sunlight, both on cloudy and sunny days. The experimental results demonstrate that, under sunlight on clear days, Kf-F-COF achieves a maximum yield of 416.56 mM g⁻¹ (Figure S42), which is comparable to the yield obtained under simulated natural light conditions in the laboratory. Furthermore, Kf-F-COF demonstrated great catalytic performance for H₂O₂ synthesis under pH-controlled condition (pH 3 to 9), in natural seawater (from the Bohai Sea in Tianjin), as well as in solutions of LiCl (1 M), NaCl (1 M), and KCl (1 M) (Figures

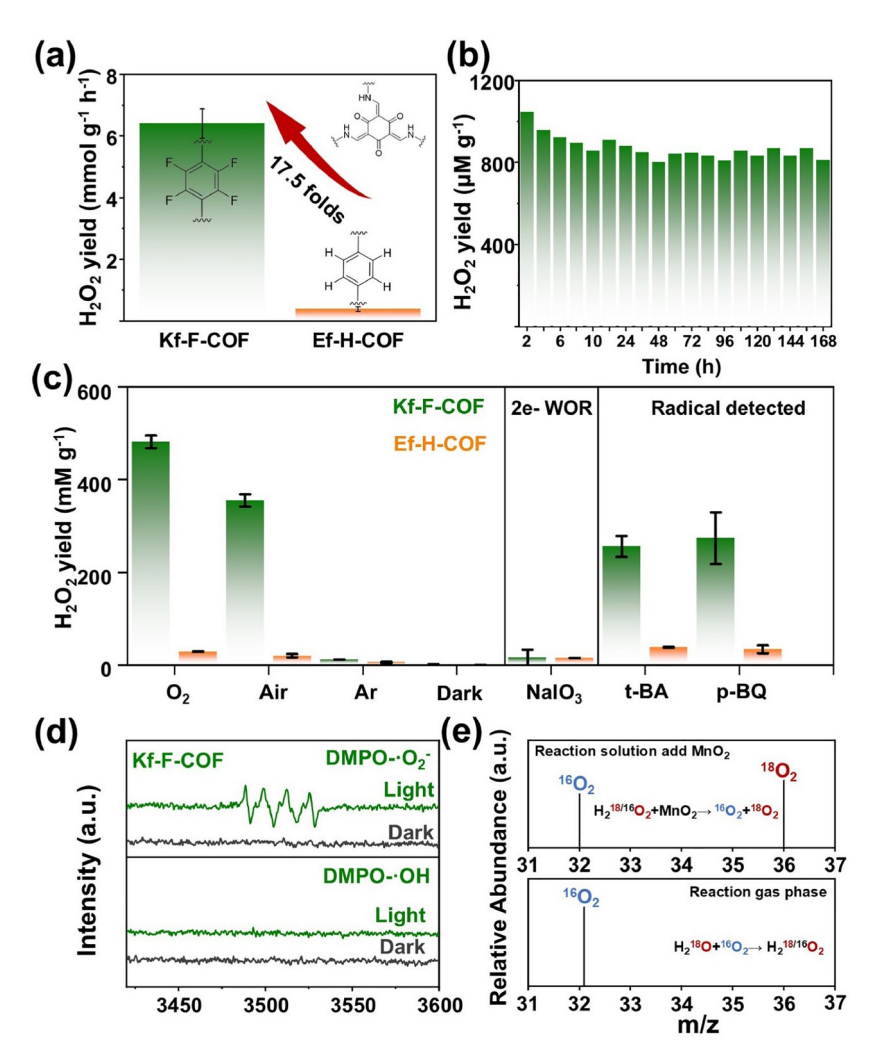


Figure 2 (Color online) (a) Photosynthesis H_2O_2 rates of Kf-F-COF and Ef-H-COF. (b) Continuous H_2O_2 production by Kf-F-COF. (c) Control experiments by Kf-F-COF and Ef-H-COF. (d) EPR spectra of Kf-F-COF. (e) MS chromatograms of the liquid products of photocatalytic $^{16}O_2/H_2^{-18}O$ reduction by Kf-F-COF.

S43–S45). These results strongly suggest that the designed Kf-F-COF holds significant potential for practical H_2O_2 generation applications.

We explored the reaction pathway for the H_2O_2 production by various control experiments. Under the condition of air atmosphere, H_2O_2 production on Kf-F-COF in the air is 355.25 mM g⁻¹, while for the Ef-H-COF is much lower as the 20.89 mM g⁻¹. In the absence of O_2 , a small amount of H_2O_2 was still produced under the catalysis of both Kf-F-COF and Ef-H-COF, with rates of 11.26 mM g⁻¹ (Kf-F-COF) and 5.21 mM g⁻¹ (Ef-H-COF), respectively. Both catalysts can facilitate water oxidation to produce H_2O_2 , with ORR being the dominant process for H_2O_2 formation. Additionally, negligible H_2O_2 production was observed in the absence of light, further confirming that light drives H_2O_2 production [25]. By bubbling argon to eliminate O_2 and adding NaIO₃ as the electron acceptor, no O_2 was detected, and only a small amount of H_2O_2 was generated

 $(9.01 \text{ mM g}^{-1} \text{ for Kf-F-COF} \text{ and } 16.08 \text{ mM g}^{-1} \text{ for Ef-H-COF})$. These results confirm that H_2O is the reactant, and O_2 is not an intermediate during the photocatalytic WOR for H_2O_2 production. Moreover, the WOR pathway for both catalysts follows a two-step process. When p-benzoquinone (pBQ) and tert-butyl alcohol (tBA) were introduced as radical scavengers, the H_2O_2 production for Kf-F-COF and Ef-H-COF was reduced, indicating that radicals are essential intermediates for H_2O_2 generation (Figure 2c).

As shown in Figure 2d, no DMPO- O_2 signal was detected under dark conditions with the addition of the catalyst, while strong electron paramagnetic resonance (EPR) signals corresponding to DMPO- O_2 were observed when Kf-F-COF and Ef-H-COF were illuminated (Figure S46) [26,27]. The electron transfer number (n) for the ORR was measured to be approximately 1.55 using the rotating disk electrode (RDE) method (Figures S47–S50). This confirms that both photocatalysts generate H_2O_2 via an O_2 intermediate through a

2e¯, two-step transfer oxygen reduction pathway $(O_2 + e^- \rightarrow O_2^-; O_2^- + e^- + H^+ \rightarrow H_2O_2)$. For the water oxidation half-reaction, no DMPO-OH signals were detected during EPR measurements with illumination (Figure S51) [28], which further supports that photogenerated holes in Kf-F-COF and Ef-H-COF are consumed via a direct 2e¯ water oxidation pathway for H_2O_2 production, as evidenced by the rotating ring-disk electrode (RRDE) results (Figures S52 and S53). These findings conclusively demonstrate that the WOR pathways of both catalysts follow a 2e¯ process without OH

as an intermediate species [29]. To trace the oxygen source in the produced $\rm H_2O_2$, we used $\rm H_2^{18}O$ with $^{16}O_2$ purging during $\rm H_2O_2$ photosynthesis (Figure S54). As shown in Figure 2e, only $^{16}O_2$ was detected both before and after the reaction, with no trace of $^{18}O_2$, indicating that no $^{18}O_2$ intermediates were produced during the $\rm H_2^{18}O$ oxidation to $\rm H_2O_2$. This confirms that the WOR process in Kf-F-COF is a 2e $^-$ transfer process, consistent with previous measurements. Notably, when the photosynthesized $\rm H_2O_2$ was decomposed by MnO_2, the resulting $\rm O_2$ consisted of approximately a 1:1 ratio of

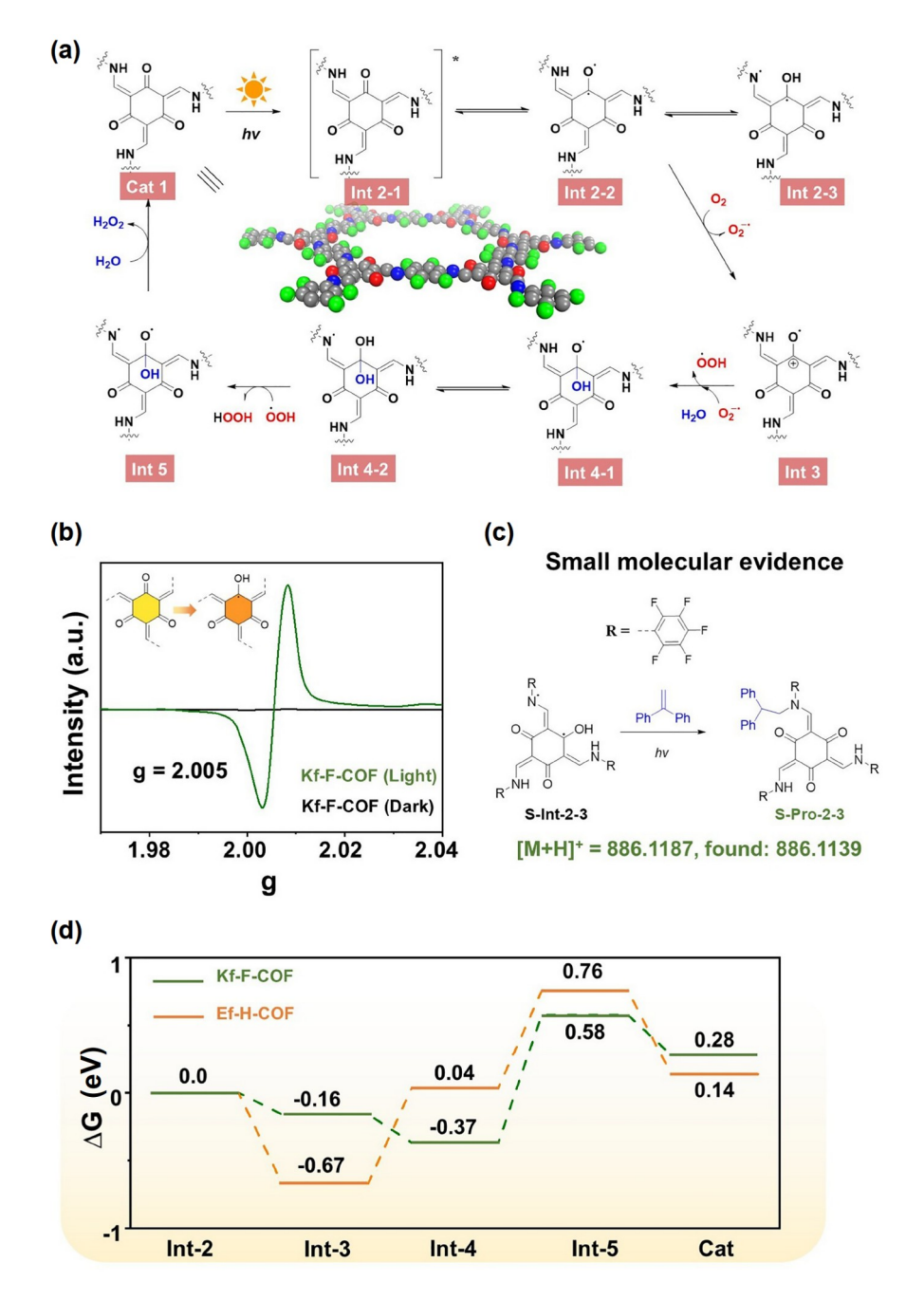


Figure 3 (Color online) (a) The proposed ORR and WOR mechanistic catalytic cycle diagrams over Kf-F-COF and Ef-H-COF. (b) EPR spectra of Kf-F-COF under dark and light conditions. (c) Schematic diagram of HR-MS for capturing small molecule free radicals. (d) Reaction profiles of Kf-F-COF and Ef-H-COF.

¹⁶O₂ and ¹⁸O₂. This suggests that both H₂O and O₂ are reactants in the photosynthesis of H₂O₂, with an atomic utilization efficiency exceeding 99% for the WOR and ORR pathways. In order to study the active site of the photocatalysts for the WOR and ORR, we used density functional theory (DFT) calculations to investigate the electron affinity characteristics of Kf-F-COF and Ef-H-COF. The analysis of the electrostatic potential (ESP) distribution revealed that the carbonyl (–C=O) groups possess distinct electron affinity properties. Under photoexcitation, these carbonyl groups exhibited a strong electron extraction capability (Figures S55 and S56).

Based on these findings and previous literature reports [30,31], we propose the following reaction mechanism (Figure 3a). Upon visible light irradiation, the keto-form structure of Kf-F-COF is excited to form Int2-1. Subsequently, the C=O group generates a diradical intermediate (Int2-2). The radical at the carbonyl site then undergoes isomerization via the adjacent imine linkage to yield Int2-3, which contains both N and C radicals. Next, molecular oxygen abstracts the carbon radical from Int2-2 to produce O_2^- , while the carbon center is oxidized to form a C^+ cation. The superoxide radical then abstracts a proton from water, forming the hydroperoxyl radical (OOH), whereas a hydroxide ion combines with the C⁺ in Int3 to produce Int4-1. This intermediate subsequently rearranges to generate Int4-2, and ·OOH converts Int4-2 into the diradical species Int-5 via aHAT process, along with the formation of one molecule of H₂O₂. Finally, the reaction of Int-5 with water produces an additional H₂O₂ molecule, thereby regenerating the initial catalyst (Cat1). EPR spectroscopy confirmed the generation of photoinduced radical species. While no signal was observed at g = 2.005 in the dark, illumination produced a distinct signal, indicating radical formation at the carbonyl sites (Figure 3b).

In addition, both hydroxymethyl (CH2OH) radicals and superoxide radicals were detected [32,33] (Figure S57), with the CH₂OH radical likely generated via C-H activation by Int-2 (Figure S58). To further probe the structure of the anion radicals, a small-molecule mimic (S-Int-2-3) was synthesized (Figures S59–S62). Upon trapping with stilbene, a single product (S-Pro-2-3) was formed (Figure 3c and Figure S63), supporting the proposed isomerization pathway. Free energy calculations were performed to assess the impact of ligand modification on H₂O₂ production. Although Ef-H-COF shows stronger O_2 activation ($\Delta G = -0.67 \text{ eV } vs.$ -0.16 eV for Kf-F-COF), the transformation from Int-3 to Int-4 in Ef-H-COF is endothermic (requiring 0.71 eV) whereas it is exothermic in Kf-F-COF ($\Delta G = -0.21 \text{ eV}$). This exothermic step in Kf-F-COF provides a thermodynamic driving force that helps facilitate the subsequent transformation to H₂O₂, despite the higher energy barrier between Int-4 and Int-5. Furthermore, the H₂O₂ formation step (Int-3 to Int-5) has a lower energy barrier in Kf-F-COF ($\Delta G = 0.95 \text{ eV}$) than in Ef-H-COF ($\Delta G = 1.43 \text{ eV}$). These results highlight the role of fluorine in enhancing carbonyl electron affinity and improving overall photocatalytic efficiency.

3 Conclusions

In summary, we developed a fluorinated covalent organic framework that features framework-bound carbonyl groups as radical-generating sites for visible-light-driven H₂O₂ production. By leveraging the structural tunability of COFs, we introduced electron-withdrawing fluorine substituents to enhance the electron affinity of carbonyl moieties, thereby promoting radical formation and stabilizing key intermediates. This design enabled efficient dual-channel photocatalysis through a radical-mediated HAT mechanism. Mechanistic investigations revealed a unique carboncentered radical pathway that drives the formation of H₂O₂ with high selectivity. Kf-F-COF demonstrated a remarkable H₂O₂ production rate of 6.42 mmol g⁻¹ h⁻¹, alongside excellent stability under natural sunlight and seawater. This work provides a framework-centered strategy for regulating radical chemistry in metal-free photocatalysts and opens new avenues for the sustainable and selective synthesis of H₂O₂.

Acknowledgements This work was supported by the National Key R&D Program of China (2022YFA1502902), the National Natural Science Foundation of China (22201209, 22271218, 22071182, 21931007, 22301235), the Shaanxi Province Young Talent Support Plan (2023SYJ28) and the Start-Up Funding of Tianjin University and Xi'an Jiaotong University.

Conflict of interest The authors declare no conflict of interest.

Supporting information The supporting information is available online at http://chem.scichina.com and http://link.springer.com/journal/11426. The supporting materials are published as submitted, without typesetting or editing. The responsibility for scientific accuracy and content remains entirely with the authors.

- Jung E, Shin H, Lee BH, Efremov V, Lee S, Lee HS, Kim J, Hooch Antink W, Park S, Lee KS, Cho SP, Yoo JS, Sung YE, Hyeon T. Nat Mater, 2020, 19: 436–442
- 2 Zhang Y, Pan C, Bian G, Xu J, Dong Y, Zhang Y, Lou Y, Liu W, Zhu Y. Nat Energy, 2023, 8: 361–371
- 3 Bryliakov KP. Chem Rev, 2017, 117: 11406-11459
- 4 Hou H, Zeng X, Zhang X. Angew Chem Int Ed, 2020, 59: 17356– 17376
- 5 Wang L, Zhang J, Zhang Y, Yu H, Qu Y, Yu J. Small, 2022, 18: 2104561
- 6 Wang L, Han C, Gao S, Jiang JX, Zhang Y. ACS Catal, 2025, 15: 5683–5693
- 7 Hao J, Tang Y, Qu J, Cai Y, Yang X, Hu J. Small, 2024, 20: 2404139
- 8 Wei S, Chang S, Li H, Fang Z, Zhu L, Xu Y. Green Chem, 2024, 26: 6382–6403
- 9 Zheng S, Fu Y, Xu X, Xu Q, Zeng G. Angew Chem Int Ed, 2025, 64:

e202503434

- 10 Tan D, Zhuang R, Chen R, Ban M, Feng W, Xu F, Chen X, Wang Q. Adv Funct Mater, 2024, 34: 2311655
- 11 Tan D, Fan X. Polymers, 2024, 16: 659
- 12 Zheng S, Ouyang Z, Liu M, Bi S, Liu G, Li X, Xu Q, Zeng G. *Carbon Neutral*, 2024, 3: 415–422
- 13 Cote AP, Benin AI, Ockwig NW, O'Keeffe M, Matzger AJ, Yaghi OM. Science, 2005, 310: 1166–1170
- 14 Yong Z, Ma T. Angew Chem Int Ed, 2023, 62: e202308980
- 15 Qian K, Guan X, Sun N, Jiang HL. Sci China Chem, 2023, 66: 436– 442
- 16 Gu YY, Wang J, Tang Q, Wei H, Ning J, Lan X, Wang X, Li X, Jia Y, Wang S, Hao L. *ACS Catal*, 2024, 14: 11262–11272
- Hu H, Tao Y, Wang D, Li C, Jiang Q, Shi Y, Wang J, Qin J, Zhou S, Kong Y. J Colloid Interface Sci. 2023, 629: 750–762
- 18 Hou Y, Zhou P, Liu F, Lu Y, Tan H, Li Z, Tong M, Ni J. Angew Chem Int Ed, 2024, 63: e202318562
- 19 Yang T, Zhang D, Kong A, Zou Y, Yuan L, Liu C, Luo S, Wei G, Yu C. Angew Chem Int Ed, 2024, 63: e202404077
- 20 Lee J, Lim H, Park J, Kim M, Jung J, Kim J, Kim I. Adv Energy Mater. 2023. 13: 2300442
- 21 Wang H, Yang C, Chen F, Zheng G, Han Q. Angew Chem Int Ed, 2022, 61: e202202328
- 22 Kandambeth S, Mallick A, Lukose B, Mane MV, Heine T, Banerjee

- R. J Am Chem Soc, 2012, 134: 19524-19527
- 23 Khayum MA, Kandambeth S, Mitra S, Nair SB, Das A, Nagane SS, Mukherjee R, Banerjee R. Angew Chem Int Ed, 2016, 55: 15604– 15608
- 24 Zhang X, Cheng S, Chen C, Wen X, Miao J, Zhou B, Long M, Zhang L. Nat Commun, 2024, 15: 2649
- Weng Z, Lin Y, Han B, Zhang X, Guo Q, Luo Y, Ou X, Zhou Y, Jiang J. *J Hazard Mater*, 2023, 448: 130869
- 26 Wu C, Teng Z, Yang C, Chen F, Yang HB, Wang L, Xu H, Liu B, Zheng G, Han Q. Adv Mater, 2022, 34: 2110266
- 27 Qian Y, Li D, Han Y, Jiang HL. J Am Chem Soc, 2020, 142: 20763– 20771
- 28 Zhou Z, Sun M, Zhu Y, Li P, Zhang Y, Wang M, Shen Y. *Appl Catal B-Environ*, 2023, 334: 122862
- 29 Li L, Lv X, Xue Y, Shao H, Zheng G, Han Q. Angew Chem Int Ed, 2024, 63: e202320218
- 30 Chi W, Dong Y, Liu B, Pan C, Zhang J, Zhao H, Zhu Y, Liu Z. *Nat Commun*, 2024, 15: 5316
- 31 Zhang X, Zhang J, Miao J, Wen X, Chen C, Zhou B, Long M. *Chem Eng J*, 2023, 466: 143085
- 32 Baran T, Dibenedetto A, Aresta M, Kruczała K, Macyk W. Chem-PlusChem, 2014, 79: 708–715
- 33 Xie S, Shen Z, Deng J, Guo P, Zhang Q, Zhang H, Ma C, Jiang Z, Cheng J, Deng D, Wang Y. *Nat Commun*, 2018, 9: 1181